Int. J. Electron. Commun. (AEÜ) 136 (2021) 153751

Contents lists available at ScienceDirect

International Journal of Electronics and Communications

journal homepage: www.elsevier.com/locate/aeue

Regular paper

SER performance of MIMO full-duplex relay system with channel estimation errors and transceivers hardware impairments

Ba Cao Nguyen [a], Phan Van Tri [b], Xuan Nam Tran [c], Le The Dung [d,e,*]

[a] Faculty of Basic Techniques, Telecommunications University, Khanh Hoa, Viet Nam
[b] Faculty of Cryptology, Ho Chi Minh Academy of Cryptography Techniques, Ho Chi Minh City, Viet Nam
[c] Advanced Wireless Communications Group, Le Quy Don Technical University, Ha Noi, Viet Nam
[d] Division of Computational Physics, Institute for Computational Science, Ton Duc Thang University, Ho Chi Minh City, Viet Nam
[e] Faculty of Electrical and Electronics Engineering, Ton Duc Thang University, Ho Chi Minh City, Viet Nam

ARTICLE INFO

Keywords:
In-band full-duplex
Multiple-input multiple-output
Channel estimation error
Transceiver hardware impairments
Imperfect self-interference cancellation
Symbol error rate

ABSTRACT

In practice, traditional wireless communication systems are often affected by various negative factors such as channel estimation errors (CEE) and transceiver hardware impairments (THI). For in-band full-duplex (FD) communication systems, besides CEE and THI impacts, imperfect self-interference cancellation will significantly degrade the system performance because of residual self-interference (RSI). This paper aims to investigate the performance of a multiple-input multiple-output (MIMO) FD relay (FDR) system in realistic scenarios where the impacts of CEE, THI, and RSI are taken into account. We mathematically derive the exact closed-form expression of symbol error rate (SER) of the considered MIMO-FDR system and validate the derived expression by Monte-Carlo simulations. Numerical results indicate that the impacts of three imperfect factors (CEE, THI, and RSI) are remarkable. Specifically, with the considered values of CEE, THI, and RSI, the impact of CEE on the SER is most substantial. Additionally, compared with the ideal system (perfect channel estimations, transceiver hardware, and self-interference cancellation), the SER of the considered system is significantly higher and goes to the error floor fast. Therefore, it is crucial to apply all solutions for reducing the CEE, THI, and RSI in the considered MIMO-FDR system.

1. Introduction

Recently, multiple-input multiple-output (MIMO) has become an advanced technique for obtaining high channel capacity and performance improvement in wireless communication systems. Various MIMO transmission techniques such as space–time codes (STC) and spatial multiplexing (SM) have been proposed and widely deployed in the current third-generation (3G) and fourth-generation (4G) systems. With the significant advantages of STC and SM, they are still the primary radio transmission techniques for the fifth-generation (5G) system [1,2]. However, due to multiple antennas for transmission and reception, MIMO systems suffer some disadvantages, such as hardware deployment difficulty and signal processing complexity. In that context, maximal ratio transmission (MRT) technique at the transmitter and maximal ratio combining (MRC) technique at the receiver were proposed to reduce the number of radio-frequency (RF) chains [3,4]. Therefore, applying MRT/MRC techniques can significantly improve the performance and diversity order of MIMO systems. At the transmitter, MRT can reach full diversity by using the optimal power allocation. Consequently, MRT is suitable for simple receiver systems, for example, the downlink of cellular communications. At the receiver, MRC can get optimum performance through the combination of weights at the receiver side [3]. Using the MRC technique helps MIMO systems achieve the maximum array gain and full diversity order. For these reasons, MRT/MRC techniques have been widely applied and analyzed in MIMO systems [5].

To satisfy the requirements of anytime and anywhere connections, high capacity and coverage of wireless networks, a lot of new communication techniques such as cognitive radios (CR), non-orthogonal multiple access (NOMA), in-band full-duplex (FD) have been proposed [6–8]. Among these techniques, FD transmission is a promising solution because it can double the spectral efficiency compared with traditional half-duplex (HD) transmission. Additionally, measurements and

* Corresponding author at: Institute for Computational Science, Ton Duc Thang University, No. 19 Nguyen Huu Tho Street, Tan Phong Ward, District 7, Ho Chi Minh City, Viet Nam.
E-mail address: lethedung@tdtu.edu.vn (L.T. Dung).

https://doi.org/10.1016/j.aeue.2021.153751
Received 5 July 2020; Accepted 8 April 2021
Available online 17 April 2021

experiments on residual self-interference (RSI) after interference cancellation demonstrated that the RSI due to FD transmission is lower than that due to CR or NOMA techniques [6]. Therefore, FD transmission is now widely investigated in both academy and industry [9,10]. However, after all self-interference cancellation (SIC) solutions, high RSI power is still a big problem that inhibits the deployment of the FD transmission mode in practice.

In the literature, various SIC architectures for FD transmission, including antenna, analog, and digital cancellation, have been proposed to obtain effective SIC [11–14]. Fortunately, the work in [12] demonstrated that SI could be suppressed up to 110 dB when three SIC domains were applied, making FD communication systems feasible in practical scenarios. In the literature, many SIC architectures and algorithms have been developed to obtain higher SIC capability for FD communication systems [11,15]. With the RSI value after all SIC solutions, FD systems can achieve higher capacity with a small performance loss than HD systems. Consequently, the FD technique is applied in different scenarios to gain FD transmission benefits compared with traditional HD transmission. Additionally, FD can be combined with various techniques such as CR, NOMA, energy harvesting (EH), spatial modulation, millimeter wave (mmWave), vehicle-to-vehicle (V2V) in a wireless communication system to utilize the advantages of these techniques [7,10,16–20].

Although FD communication systems were considered in various scenarios, the critical issue for analyzing these systems is the impact of RSI after SIC on the performance parameters such as outage probability (OP), symbol error rate (SER), and ergodic capacity (EC). In [17,21], the authors exploited of FD technique into V2V communication systems. The OP and SER of FD relay (FDR) single-antenna systems using both decode-and-forward (DF) and amplify-and-forward (AF) were analyzed over double Rayleigh fading channels. Their results demonstrated that, besides the impact of the RSI, the double Rayleigh fading channel has a significant effect on the OP and SER of V2V communication systems. To obtain a higher capacity for wireless networks, the works in [16,22] used FDR in a NOMA system. They derived the exact expressions of OP and EC of two NOMA users to investigate the impact of the RSI on this system. On the other hand, multiple antennas, together with other techniques such as MRC/MRT, spatial modulation, transmit antenna selection (TAS), were exploited in [20,23–26] to enhance the system performance. Their results indicated that multiple antennas could significantly mitigate the effect of the RSI on OP and SER of FDR systems. Moreover, using optimal power allocation for FD transmission mode can remarkably reduce the OP and SER [20,27].

Besides the sole impact of the RSI on the OP, SER, and EC of FDR systems, the joint effect of channel estimation error (CEE) and RSI was also considered to investigate FDR systems' performance in realistic scenarios [28,29]. Under the joint impact of CEE and RSI, the OP and SER of the FDR systems go to the error floor faster. At the error floor, the OP and SER of FDR systems are significantly higher than those in the case of perfect CSI. On the other hand, the combined impact of transceiver hardware impairment (THI) and RSI has also been considered in the literature because THI often exists in wireless systems, especially for low-cost devices such as relays [27,30–34]. The results in these works demonstrated that, when THI is considered, the computational complexity for calculating OP, SER, and EC is considerably higher compared with the ideal hardware systems, especially for calculating SER. Thus, most of the works considering the THI only derived OP expression for analyzing the system performance. In the case of THI, the single-antenna systems soon go to the error floor, specifically for high data transmission rate systems. In this context, the usage optimal power allocation for FDR or multiple antennas with MRC/MRT can significantly reduce the impact of THI and RSI and improve the system performance [24,27,33]. For the ease of readability, previous works on MIMO-FDR systems that considered the individual and combined effects of CEE, THI, and RSI are summarized in Table 1.

It is evident from the above discussions that FDR systems have been widely investigated in different scenarios because of FD and other techniques' benefits. Additionally, realistic FDR systems suffer from the RSI and many other negative factors such as CEE and THI. Therefore, neglecting CEE and THI when analyzing the FDR systems may result in insufficient evaluations and conclusions. Furthermore, using multiple antennas with MRC/MRT techniques provides lower OP and SER of FDR systems because MRT/MRC are easy signal processing techniques but can maximize the signal-to-noise ratio (SNR) at the receiver. Also, SER is an essential parameter for evaluating the system performance; however, it has not been studied in the literature for the MIMO-FDR system with CEE, THI, and RSI. Motivated by this observation, in this paper, we mathematically analyze the performance of a MIMO-FDR system under the impact of three negative factors, i.e., CEE, THI, and RSI by deriving exact closed-form expression of SER. Thanks to the usage of FD transmission, the number of connected devices can be doubled. Hence, our considered MIMO-FDR system is suitable for various applications which require massive connections such as low delay communications, small and dense cells [6,8,12]. Also, by taking CEE, THI, and RSI into consideration, the considered MIMO-FDR system is more realistic. The main contributions of the paper are summarized as follows.– We consider a MIMO-FDR system under the impact of CEE, THI, and RSI. Specifically, CEE occurs in both S–R and R–D communication channels, THI is in all nodes in the system, and RSI still exists at the FDR node after all SIC techniques.– We calculate the received signals at the relay and destination with CEE, THI, and RSI. Then, the expression of the signal-to-interference-plus-noise-and-distortion ratio (SINDR) of the considered MIMO-FDR system is derived for further analysis. From the expression of the SINDR, we obtain the exact closed-form expression of SER of the considered MIMO-FDR system with MRT/MRC techniques over Rayleigh fading channels. Monte-Carlo simulations are conducted to demonstrate the exactness of our mathematical analysis.– We compare the SER of the considered system with that of the ideal system. Based on these comparisons, we show the impacts of one or two or three negative factors on SER of the considered MIMO-FDR system. Notably, under the influences of three negative factors, SER reduces fast in the low SNR regime and goes to the error floor in the high SNR regime. Therefore, besides applying various solutions to decrease the effect of three negative factors, we should use appropriate transmission power for the system to save energy and avoid the error floor.

Table 1
Summary of previous works on MIMO-FDR systems with CEE, THI, and RSI.

References	Problem	Obtained expressions
[16,17,20–26]	RSI	SER [20]; EC [23,25]; OP and SER [17,21,24,26]; OP and EC [16,22]
[28,29]	CEE and RSI	OP [29]; OP and SER [28]
[27,30–32,34]	THI and RSI	EC [30,32]; OP and EC [31]; OP and SER [27,34]

The rest of this paper is organized as follows. Section 2 presents the system model where CEE, THI, and RSI models are presented in detail. Section 3 focuses on mathematical analysis of the system performance by deriving the closed-form expression of SER of the considered MIMO-FDR system. Section 4 provides numerical results and discussion. Finally, Section 5 concludes this paper.

2. System Model

Fig. 1 illustrates the block diagram of a MIMO-FDR system with three imperfect factors (CEE, THI, and RSI). In the considered system, source (S) and destination (D) are single-antenna devices, while relay (R) is a multi-antenna device with N_r reception antennas and N_t transmission antennas. Additionally, S and D use traditional HD transmission mode while R exploits FD transmission mode. Signals are transmitted from S to D via the assistance of R, which uses the decode-and-forward (DF) protocol. As can be seen from Fig. 1, the considered MIMO-FDR system is

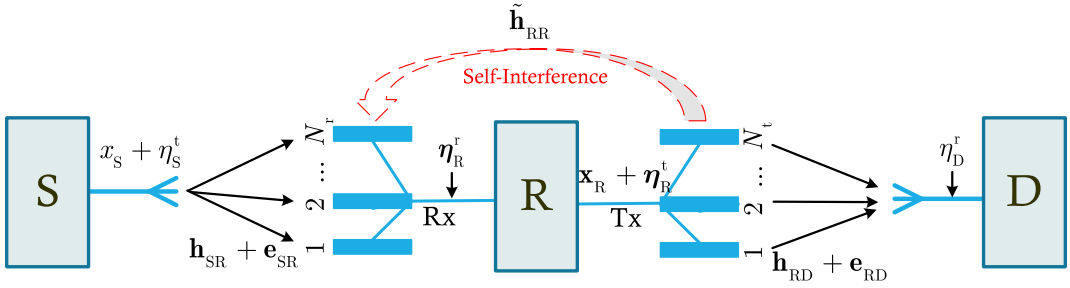

Fig. 1. Block diagram of the considered MIMO-FDR system with CEE, THI, and RSI.

affected by three imperfect factors, i.e., CEE, THI, and RSI. In the following parts, we will indicate these factors in the system.

2.1. Channel Model

As presented in Fig. 1, the channel coefficients of S–R and R–D links are denoted by $\mathbf{h}_{\mathrm{SR}}$ and $\mathbf{h}_{\mathrm{RD}}$, respectively, which follow Rayleigh distributions. Additionally, the direct link between S and D does not exist because of significant separation and a strong shadowing effect. Moreover, the SI occurring from transmission antennas to reception antennas of R due to FD mode is denoted by $\tilde{\mathbf{h}}_{\mathrm{RR}}$.

2.1.1. Channel Estimation Error

Before signal transmission, channel estimation is performed by using pilot symbols. The transmitters (S and R) transmit pilot symbols. Then, through monitoring the received signals, the receivers (R and D) immediately feedback the transmit weights for MRC/MRT techniques corresponding with the transmission antennas and the instantaneous signal-to-interference-plus-noise-and-distortion ratio (SINDR) at the receiver side. To obtain the CSI, the receivers (R and D) use the minimum-mean-square-error (MMSE) method to estimate the channel coefficients of communication links from S to R and from R to D [35]. Therefore, the S – R and R – D channels in the case of CEE are expressed as

$$\widehat{\mathbf{h}}_{ij} = \mathbf{h}_{ij} + \mathbf{e}_{ij}, \tag{1}$$

where $ij \in \{\mathrm{SR}; \mathrm{RD}\}$; $\mathbf{h}_{ij}$ and $\mathbf{e}_{ij}$ are the channel estimation vector and the channel estimation error vector, respectively. Herein, all elements of the channel estimation vector follow Rayleigh distributions while all elements of the channel estimation error vector follow complex Gaussian distributions with zero means and variances of $\sigma_{e_{ij}}^2$ [29].

2.1.2. RSI Model

As aforementioned, although the FD transmission mode can double the spectral efficiency, the self-interference (SI) from transmission antennas to reception antennas significantly degrades FD systems' performance. Therefore, all self-interference cancellation (SIC) solutions in antenna, analog, and digital domains should be applied at R to suppress the SI power. Initially, in the antenna domain, R uses absorptive shielding, directional isolation, and cross-polarization to suppress the SI power from the transmitting antennas to the receiving antennas of R. It is noted that, although R can use shared-antennas for both transmitting and receiving signals in practice, using SIC in antenna domain is more effective when separate antennas are used as in the considered MIMO-FDR system [13]. After SIC in the antenna domain, R suppresses SI in the analog and digital domain by applying signal processing methods. By exploiting the architectures for SIC in both analog and digital domain [11,13,36], R can subtract SI from the received signals. However, due to imperfect SI channel estimation and hardware, R cannot remove SI completely. The RSI still exists in R and dramatically impacts the system performance. Furthermore, as presented in the literature, these SIC solutions allow a significant reduction in the impact of the SI from the direct path. The report in [12] stated that an attenuation level of up to 50 dB in the antenna domain is possible if appropriate solutions are used. However, the impact of the SI channel is mainly due to the reflected paths. In this case, the channel gain of the direct path no longer dominates the channel gains of reflected paths. Since the direct and reflected paths are statistically independent, using the central limit theorem, the overall path gain of the SI channel can be described as a complex Gaussian variable [12,36]. Additionally, researches and measurements about RSI also indicated that RSI follows Gaussian distribution after using all SIC techniques [11,12,36–38].

2.1.3. THI Model

In practice, the transmitted and received signals of wireless systems are distorted by the THI. Generally, the sources of THI are phase noise (PN), in-phase/quadrature (I/Q) imbalance, and nonlinearities of various electronic components such as analog-to-digital (A/D) and digital-to-analog (D/A) converters, mixers, and amplifiers (high power amplifier (HPA) in the transmitter and low-noise amplifier (LNA) in the receiver) [39–42].

First, PN is a common factor that limits wireless systems' performance, especially for low-cost wireless systems operating with high carrier frequencies because their oscillators cannot provide sufficient working stability [39]. PN is challenging to remove entirely after various solutions. These include using digital signal processing in the baseband part of the receiver, performing data symbol estimation from the previous iteration, and applied. Second, I/Q imbalance refers to the phase and amplitude imbalance between the I and Q signals. Different data-aided estimation and compensation approaches such as preamble design, iterative transmitter, and receiver IQ imbalance estimation were proposed to reduce the impacts of I/Q imbalance at both transmitter and receiver. However, it is impossible to achieve perfect matching between the I and Q branch of the quadrature transmitter/receiver due to the limited accuracy in implementing the radio frequency (RF) front-end [39]. Third, nonlinearities of electronic components often come from the A/D and D/A converters, mixers, and amplifiers, e.g., HPA in the transmitter and LNA in the receiver [39,43]. Various techniques have been applied to overcome the influence of nonlinearities. For example, for MIMO-OFDM systems, two conventional solutions that can overcome the nonlinearity problem are either using highly linear components or applying a large input power backoff (BO). As a result, that the signals can experience the linear part of the transfer of the components [39].

As presented above, various factors cause the THI in wireless systems. Consequently, many compensation methods should be applied to deal with these factors individually. Also, various works considered only IQ imbalance [44], only nonlinear distortion effect [43], or aggregate transceiver impairment of all factors [31,40–42]. However, theoretical research and practical measurement often model the combined impact of all impairments, which is useful for system designers [39,45]. A common assumption considers that the distortion noises at the transmitter and the receiver are Gaussian distributed with their average power is proportional to the average signal power [31,34,40–42]. This assumption is based on the central limit theorem (CLT) and validated by measurement results [39]. In this paper, the THI is also considered as a

Gaussian distribution. Moreover, it is worth noticing that THI is a major factor that causes CEE and RSI in the considered MIMO-FDR system. Specifically, higher THI leads to higher CEE and RSI. However, THI, CEE, and RSI are often modeled and measured independently [12,36,39,46,47]. Therefore, in this paper, we assume that they are independent.

From Fig. 1, the distortion noises in the transmitters S and R are $\eta_{\rm S}^{\rm t}$ and $\boldsymbol{\eta}_{\rm R}^{\rm t}$, respectively, where $\eta_{\rm S}^{\rm t} \sim \mathcal{CN}(0, (k_{\rm S}^{\rm t})^2 P_{\rm S}), \boldsymbol{\eta}_{\rm R}^{\rm t} \sim \mathcal{CN}(0, (k_{\rm R}^{\rm t})^2 \frac{P_{\rm R}}{N_{\rm t}})$, with $k_{\rm S}^{\rm t}$ and $k_{\rm R}^{\rm t}$ are, respectively, the HI levels at the transmitters S and R; $P_{\rm S}$ and $\frac{P_{\rm R}}{N_{\rm t}}$ are, respectively, the average transmission power per one antenna of S and R. In the receivers, the distortion noises are $\boldsymbol{\eta}_{\rm R}^{\rm r}$ and $\eta_{\rm D}^{\rm r}$ for receivers R and D, respectively, where $\boldsymbol{\eta}_{\rm R}^{\rm r} \sim \mathcal{CN}(0, \|\widehat{\mathbf{h}}_{\rm SR}\|^2 (k_{\rm R}^{\rm r})^2 P_{\rm S})$, $\eta_{\rm D}^{\rm r} \sim \mathcal{CN}(0, \|\widehat{\mathbf{h}}_{\rm RD}\|^2 (k_{\rm D}^{\rm r})^2 \frac{P_{\rm R}}{N_{\rm t}})$, with $k_{\rm R}^{\rm r}$ and $k_{\rm D}^{\rm r}$ are, respectively, the HI levels at the receivers R and D.

It is noted that applying all SIC techniques in the case of THI has been investigated and measured in the literature [11–15]. In particular, the novel digital SIC technique proposed in [11] significantly reduces the SI signal power and the associated transceiver impairments. Besides, although both linear and non-linear effects were considered, the design and implementation of an FD radio in [12] could still mitigate up to 110 dB SI power when all SIC techniques were applied. Therefore, although THI reduces the SIC capability of FD devices, current techniques can suppress SI to the noise floor [13–15]. The variance of channel estimation error may be reduced when the transmission power of S and R increases. Unfortunately, the levels of HI and RSI may increase with the transmission power of S and R. However, most of the works investigating the effects of CEE, THI, and RSI considered them as constants [28,29,31,38,40,41]. Similarly, we also consider these factors as constants in this paper.

2.2. Signal Model

Based on all the above definitions, the received signal at R of the considered MIMO-FDR system with CEE and THI is expressed as

$$\mathbf{y}_{\rm R} = \widehat{\mathbf{h}}_{\rm SR}(x_{\rm S} + \eta_{\rm S}^{\rm t}) + \boldsymbol{\eta}_{\rm R}^{\rm r} + \widetilde{\mathbf{h}}_{\rm RR}(\mathbf{x}_{\rm R} + \boldsymbol{\eta}_{\rm R}^{\rm r}) + \mathbf{z}_{\rm R}, \tag{2}$$

where $x_{\rm S}$ is the desired transmit signal from S; $\widehat{\mathbf{h}}_{\rm SR} = [\widehat{h}_{\rm S1}\ \widehat{h}_{\rm S2} \dots \widehat{h}_{{\rm S}N_{\rm r}}]^T$ is the channel vector from the transmission antenna of S to $N_{\rm r}$ reception antennas of R; $\widetilde{\mathbf{h}}_{\rm RR}$ is the SI channel matrix before SIC; $\mathbf{x}_{\rm R} = [x_1\ x_2 \dots x_{N_{\rm t}}]^T$ is the transmitted signal vector at $N_{\rm t}$ transmission antennas of R; $\mathbf{z}_{\rm R}$ is the Gaussian noise vector at R whose elements have zero means and variances of $\sigma_{\rm R}^2$, i.e., $\mathbf{z}_{\rm R} \sim \mathcal{CN}(0, \sigma_{\rm R}^2)$.

After receiving signals, R applies various SIC solutions. Then, the RSI after these SIC techniques (denoted by $\mathbf{I}_{\rm R}$) follows Gaussian distribution[1], i.e., $\mathbf{I}_{\rm R} \sim \mathcal{CN}(0, \sigma_{\rm RSI}^2)$, where $\sigma_{\rm RSI}^2 = l^2 P_{\rm R}$ with l is RSI level at R [12,19,20,48].

Now, the received signal at R can be rewritten as

$$\mathbf{y}_{\rm R} = \widehat{\mathbf{h}}_{\rm SR}(x_{\rm S} + \eta_{\rm S}^{\rm t}) + \boldsymbol{\eta}_{\rm R}^{\rm r} + \mathbf{I}_{\rm R} + \mathbf{z}_{\rm R}. \tag{3}$$

Applying (1), (3) becomes

$$\mathbf{y}_{\rm R} = \widehat{\mathbf{h}}_{\rm SR} x_{\rm S} + \widehat{\mathbf{h}}_{\rm SR}\eta_{\rm S}^{\rm t} + \boldsymbol{\eta}_{\rm R}^{\rm r} + \mathbf{I}_{\rm R} + \mathbf{z}_{\rm R} = \mathbf{h}_{\rm SR} x_{\rm S} + \widehat{\mathbf{h}}_{\rm SR}\eta_{\rm S}^{\rm t} + \boldsymbol{\eta}_{\rm R}^{\rm r} + \mathbf{e}_{\rm SR} x_{\rm S} + \mathbf{I}_{\rm R} + \mathbf{z}_{\rm R}. \tag{4}$$

Next, R decodes the received signals, recodes and forwards them to D. The received signals at destination D is

$$y_{\rm D} = \widehat{\mathbf{h}}_{\rm RD}(\mathbf{x}_{\rm R} + \boldsymbol{\eta}_{\rm R}^{\rm t}) + \eta_{\rm D}^{\rm r} + z_{\rm D} = \mathbf{h}_{\rm RD}\mathbf{x}_{\rm R} + \widehat{\mathbf{h}}_{\rm RD}\boldsymbol{\eta}_{\rm R}^{\rm t} + \eta_{\rm D}^{\rm r} + \mathbf{e}_{\rm RD}\mathbf{x}_{\rm R} + z_{\rm D}, \tag{5}$$

where $\widehat{\mathbf{h}}_{\rm RD} = [\widehat{h}_{1\rm D}\ \widehat{h}_{2\rm D} \dots \widehat{h}_{N_{\rm t}\rm D}]$ is the channel vector from $N_{\rm t}$ transmission antennas of R to the reception antenna of D; $z_{\rm D} \sim \mathcal{CN}(0, \sigma_{\rm D}^2)$ is the Gaussian noise at D.

Based on (4) and (5), the SINDR at R ($\gamma_{\rm R}$) and D ($\gamma_{\rm D}$) are, respectively, calculated as

$$\gamma_{\rm R} = \frac{\|\mathbf{h}_{\rm SR}\|^2 P_{\rm S}}{\|\widehat{\mathbf{h}}_{\rm SR}\|^2 (k_{\rm S}^{\rm t})^2 P_{\rm S} + \|\widehat{\mathbf{h}}_{\rm SR}\|^2 (k_{\rm R}^{\rm r})^2 P_{\rm S} + \sigma_{e_{\rm SR}}^2 P_{\rm S} + \sigma_{\rm RSI}^2 + \sigma_{\rm R}^2} = \frac{\|\mathbf{h}_{\rm SR}\|^2 P_{\rm S}}{\|\widehat{\mathbf{h}}_{\rm SR}\|^2 k_{\rm SR}^2 P_{\rm S} + \sigma_{e_{\rm SR}}^2 P_{\rm S} + \sigma_{\rm RSI}^2 + \sigma_{\rm R}^2} = \frac{\|\mathbf{h}_{\rm SR}\|^2 P_{\rm S}}{\|\mathbf{h}_{\rm SR}\|^2 k_{\rm SR}^2 P_{\rm S} + \sigma_{e_{\rm SR}}^2 P_{\rm S}(1 + k_{\rm SR}^2) + \sigma_{\rm RSI}^2 + \sigma_{\rm R}^2}, \tag{6}$$

$$\gamma_{\rm D} = \frac{\|\mathbf{h}_{\rm RD}\|^2 \frac{P_{\rm R}}{N_{\rm t}}}{\|\widehat{\mathbf{h}}_{\rm RD}\|^2 (k_{\rm R}^{\rm r})^2 \frac{P_{\rm R}}{N_{\rm t}} + \|\widehat{\mathbf{h}}_{\rm RD}\|^2 (k_{\rm D}^{\rm r})^2 \frac{P_{\rm R}}{N_{\rm t}} + \sigma_{e_{\rm RD}}^2 P_{\rm R} + \sigma_{\rm D}^2} = \frac{\|\mathbf{h}_{\rm RD}\|^2 \frac{P_{\rm R}}{N_{\rm t}}}{\|\widehat{\mathbf{h}}_{\rm RD}\|^2 k_{\rm RD}^2 \frac{P_{\rm R}}{N_{\rm t}} + \sigma_{e_{\rm RD}}^2 P_{\rm R} + \sigma_{\rm D}^2} = \frac{\|\mathbf{h}_{\rm RD}\|^2 P_{\rm R}}{\|\mathbf{h}_{\rm RD}\|^2 k_{\rm RD}^2 P_{\rm R} + N_{\rm t}\sigma_{e_{\rm RD}}^2 P_{\rm R}(1 + k_{\rm RD}^2) + N_{\rm t}\sigma_{\rm D}^2}, \tag{7}$$

where $k_{\rm SR}^2 = (k_{\rm S}^{\rm t})^2 + (k_{\rm R}^{\rm r})^2, k_{\rm RD}^2 = (k_{\rm R}^{\rm t})^2 + (k_{\rm D}^{\rm r})^2$ are, respectively, the aggregated HI levels from transmitter S ($k_{\rm S}^{\rm t}$) and receiver R ($k_{\rm R}^{\rm r}$) and from transmitter R ($k_{\rm R}^{\rm t}$) and receiver D ($k_{\rm D}^{\rm r}$).

3. Performance Analysis

The SER of the considered MIMO-FDR system under the impact of CEE and THI with coherent detection is computed as [49]

$$\text{SER} = a\mathbb{E}\{Q(\sqrt{b\gamma})\} = \frac{a}{\sqrt{2\pi}}\int_0^\infty F\left(\frac{t^2}{b}\right)\exp\left(-\frac{t^2}{2}\right)dt, \tag{8}$$

where (a, b) is a pair of parameters whose values depend on specific modulation types, e.g. $(a, b) = (1, 2)$ and $(a, b) = (2, 1)$ for binary phase-shift keying (BPSK) and 4-quadrature amplitude modulation (4-QAM)

[1] Besides being modeled as a complex Gaussian distribution, RSI can be characterized by several distributions such as Rician, Rayleigh, and Nakagami [28,36,29]. These distributions are often used to emphasize the modeling of the RSI. Although the impact of Rician/Rayleigh/Nakagami distributed RSI on system performance is similar to that of Gaussian distributed RSI, using Rician, Rayleigh, or Nakagami to model the RSI increases the computational complexity.

modulations, respectively; γ is the end-to-end SINDR; $F(.)$ is the CDF of the end-to-end SINDR of the considered MIMO-FDR system; $Q(z) \triangleq \frac{1}{\sqrt{2\pi}}\int_z^\infty \exp\left(-\frac{u^2}{2}\right)du$ is the Gaussian function.

Let $x = \frac{t^2}{b}$, (8) is rewritten as

$$\text{SER} = \frac{a\sqrt{b}}{2\sqrt{2\pi}}\int_0^\infty \frac{\exp\left(-\frac{bx}{2}\right)}{\sqrt{x}}F(x)dx. \tag{9}$$

From (9), the SER of the considered MIMO-FDR system with CEE and THI is given in the following Theorem.

Theorem. Under the impact of CEE and THI, the closed-form expression of SER of the considered MIMO-FDR system is calculated as

$$\text{SER} = \frac{a\sqrt{b}}{2\sqrt{2\pi}}\left[\sqrt{\frac{2\pi}{b}} - \frac{\pi}{2M\lambda^2}\sum_{m=1}^{M}\sum_{i=0}^{N_t-1}\sum_{j=0}^{N_t-1}\frac{\Theta^i\Psi^j\Lambda^{i+j-\frac{1}{2}}\sqrt{1-\phi_m^2}}{i!j!(1-k_{\text{SR}}^2\Lambda)^i(1-k_{\text{RD}}^2\Lambda)^j} \times \exp\left(-\frac{b\Lambda}{2} - \frac{\Theta\Lambda}{1-k_{\text{SR}}^2\Lambda} - \frac{\Psi\Lambda}{1-k_{\text{RD}}^2\Lambda}\right)\right], \tag{10}$$

where $\Theta = \frac{\sigma_{e_{\text{SR}}}^2 P_{\text{S}}(1+k_{\text{SR}}^2)+\sigma_{\text{RSI}}^2+\sigma_{\text{R}}^2}{\Omega_{\text{SR}}P_{\text{S}}}$; $\Psi = \frac{N_t[\sigma_{e_{\text{RD}}}^2 P_{\text{R}}(1+k_{\text{RD}}^2)+\sigma_{\text{D}}^2]}{\Omega_{\text{RD}}P_{\text{R}}}$; $\frac{1}{\lambda^2} = \min\left(\frac{1}{k_{\text{RD}}^2}, \frac{1}{k_{\text{SR}}^2}\right)$; $\Lambda = \frac{1}{2\lambda^2}(1+\phi_m)$; $\phi_m = \cos\left(\frac{(2m-1)\pi}{2M}\right)$; Ω_{SR} and Ω_{RD} denote the average channel gains of S–R and R–D channels, respectively; M is a complexity-accuracy trade-off parameter.

Proof. As defined in (9), the SER is computed through the CDF of the end-to-end SINDR, $F(x)$. Therefore, we first calculate $F(x)$ of the considered MIMO-FDR system.

As presented in [49], $F(x)$ is computed as

$$F(x) = \Pr\{\gamma < x\}. \tag{11}$$

Due to DF protocol is applied at R, the end-to-end SINDR, γ, of the considered MIMO-FDR system is expressed as

$$\gamma = \min\{\gamma_{\text{R}}, \gamma_{\text{D}}\}, \tag{12}$$

where γ_{R} and γ_{D} are, respectively, the SINDRs at R and D, and are given in (6) and (7).

Replacing (12) into (11), we have

$$F(x) = \Pr\{\gamma < x\} = \Pr\{\min\{\gamma_{\text{R}}, \gamma_{\text{D}}\} < x\} = \Pr\{(\gamma_{\text{R}} < x) \cup (\gamma_{\text{D}} < x)\}. \tag{13}$$

Since $\Pr\{\gamma_{\text{R}} < x\}$ and $\Pr\{\gamma_{\text{D}} < x\}$ are two independent events, the above probability is now calculated as

$$F(x) = \Pr\{\gamma_{\text{R}} < x\} + \Pr\{\gamma_{\text{D}} < x\} - \Pr\{\gamma_{\text{R}} < x\}\Pr\{\gamma_{\text{D}} < x\}. \tag{14}$$

To obtain the closed-form expression of (14), two probabilities, i.e., $\Pr\{\gamma_{\text{R}} < x\}$and $\Pr\{\gamma_{\text{D}} < x\}$, are needed.

It is noticed that, at the transmitter side of MIMO systems, MRT provides maximum array gain while other techniques such as transmit antenna selection (TAS) achieves limited array gain [3,4]. Also, at the receiver side, MRC performs best among different combining techniques such as selection combining (SC), switch and stay combining (SSC), threshold combining (TC), and equal-gain combining (EGC) [3,4,50]. Therefore, in this paper, we apply MRC/MRT techniques at the MIMO-FD relay R. Then, all reception and transmission antennas of R are used for receiving and transmitting signals, respectively. Consequently, the probability $\Pr\{\gamma_{\text{R}} < x\}$ is expressed as

$$\Pr\{\gamma_{\text{R}} < x\} = \Pr\left\{\frac{\|\mathbf{h}_{\text{SR}}\|^2 P_{\text{S}}}{\|\mathbf{h}_{\text{SR}}\|^2 k_{\text{SR}}^2 P_{\text{S}} + \sigma_{e_{\text{SR}}}^2 P_{\text{S}}(1+k_{\text{SR}}^2) + \sigma_{\text{RSI}}^2 + \sigma_{\text{R}}^2} < x\right\}, \tag{15}$$

or can be rewritten as

$$\Pr\{\gamma_{\text{R}} < x\} = \Pr\left\{\|\mathbf{h}_{\text{SR}}\|^2 P_{\text{S}}(1-k_{\text{SR}}^2 x) < x\left[\sigma_{e_{\text{SR}}}^2 P_{\text{S}}(1+k_{\text{SR}}^2) + \sigma_{\text{RSI}}^2 + \sigma_{\text{R}}^2\right]\right\}. \tag{16}$$

To derive the closed-form expression from (16), there are two cases that need to consider, i.e., $1-k_{\text{SR}}^2 x \leqslant 0$ and $1-k_{\text{SR}}^2 x > 0$.

First, when $1-k_{\text{SR}}^2 x \leqslant 0$ or $x \geqslant 1/k_{\text{SR}}^2$, $\|\mathbf{h}_{\text{SR}}\|^2 P_{\text{S}}(1-k_{\text{SR}}^2 x) \leqslant 0$ and $x\left[\sigma_{e_{\text{SR}}}^2 P_{\text{S}}(1+k_{\text{SR}}^2) + \sigma_{\text{RSI}}^2 + \sigma_{\text{R}}^2\right] \rangle 0$. Therefore, the probability in (16) is always true, that means $\Pr\{\gamma_{\text{R}} < x\} = 1$when $x \geqslant 1/k_{\text{SR}}^2$.

Second, when $1-k_{\text{SR}}^2 x > 0$ or $x < \frac{1}{k_{\text{SR}}^2}$, (16) becomes

$$\Pr\{\gamma_{\text{R}} < x\} = \Pr\left\{\|\mathbf{h}_{\text{SR}}\|^2 < \frac{x\left[\sigma_{e_{\text{SR}}}^2 P_{\text{S}}(1+k_{\text{SR}}^2) + \sigma_{\text{RSI}}^2 + \sigma_{\text{R}}^2\right]}{P_{\text{S}}(1-k_{\text{SR}}^2 x)}\right\}. \tag{17}$$

For MRC/MRT techniques, the cumulative distribution function (CDF, $F(.)$) and the probability density function (PDF, $f(.)$) of $\|\mathbf{h}_{\text{SR}}\|^2 = |h_{\text{S1}}|^2 + |h_{\text{S2}}|^2 + \ldots + |h_{\text{SN}_t}|^2$, are respectively given by [26]

$$F_{\|\mathbf{h}_{\text{SR}}\|^2}(x) = 1 - \exp\left(-\frac{x}{\Omega_{\text{SR}}}\right)\sum_{i=0}^{N_t-1}\frac{1}{i!}\left(\frac{x}{\Omega_{\text{SR}}}\right)^i, \quad x \geqslant 0, \tag{18}$$

$$f_{\|\mathbf{h}_{\text{SR}}\|^2}(x) = \frac{x^{N_t-1}}{\Omega_{\text{SR}}^{N_t}\Gamma(N_t)}\exp\left(-\frac{x}{\Omega_{\text{SR}}}\right), \quad x \geqslant 0, \tag{19}$$

where $\Omega_{\text{SR}} = \mathbb{E}\{|h_{\text{S1}}|^2\} = \mathbb{E}\{|h_{\text{S2}}|^2\} = \cdots = \mathbb{E}\{|h_{\text{SN}_t}|^2\}$ denotes the average channel gain of S–R channels, $\mathbb{E}$ refers to the expectation operator; $\Gamma(.)$ is the gamma function [51].

Using (18), (17) is now expressed as

$$\begin{aligned}\Pr\{\gamma_{\text{R}} < x\} &= F_{\|\mathbf{h}_{\text{SR}}\|^2}\left(\frac{x\left[\sigma_{e_{\text{SR}}}^2 P_{\text{S}}(1+k_{\text{SR}}^2) + \sigma_{\text{RSI}}^2 + \sigma_{\text{R}}^2\right]}{P_{\text{S}}(1-k_{\text{SR}}^2 x)}\right) \\ &= 1 - \exp\left(-\frac{x\left[\sigma_{e_{\text{SR}}}^2 P_{\text{S}}(1+k_{\text{SR}}^2) + \sigma_{\text{RSI}}^2 + \sigma_{\text{R}}^2\right]}{\Omega_{\text{SR}}P_{\text{S}}(1-k_{\text{SR}}^2 x)}\right) \\ &\quad \times \sum_{i=0}^{N_t-1}\frac{1}{i!}\left(\frac{x\left[\sigma_{e_{\text{SR}}}^2 P_{\text{S}}(1+k_{\text{SR}}^2) + \sigma_{\text{RSI}}^2 + \sigma_{\text{R}}^2\right]}{\Omega_{\text{SR}}P_{\text{S}}(1-k_{\text{SR}}^2 x)}\right)^i \\ &= 1 - \exp\left(-\frac{\Theta x}{1-k_{\text{SR}}^2 x}\right)\sum_{i=0}^{N_t-1}\frac{1}{i!}\left(\frac{\Theta x}{1-k_{\text{SR}}^2 x}\right)^i,\end{aligned} \tag{20}$$

where Θ was defined in the previous Theorem.

After combining two previous cases, the closed-form expression of $\Pr\{\gamma_{\text{R}} < x\}$is presented as

$$\Pr\{\gamma_{\text{R}} < x\} = \begin{cases} 1 - \exp\left(-\frac{\Theta x}{1-k_{\text{SR}}^2 x}\right)\sum_{i=0}^{N_t-1}\frac{1}{i!}\left(\frac{\Theta x}{1-k_{\text{SR}}^2 x}\right)^i, & x < \frac{1}{k_{\text{SR}}^2}, \\ 1, & x \geqslant \frac{1}{k_{\text{SR}}^2}. \end{cases} \tag{21}$$

Similarly, the closed-form expression of $\Pr\{\gamma_{\text{D}} < x\}$is given by

$$\Pr\{\gamma_D < x\} = \begin{cases} 1 - \exp\left(-\dfrac{\Psi x}{1-k_{RD}^2 x}\right)\displaystyle\sum_{j=0}^{N_t-1}\frac{1}{j!}\left(\frac{\Psi x}{1-k_{RD}^2 x}\right)^j, & x < \dfrac{1}{k_{RD}^2}, \\ 1, & x \geqslant \dfrac{1}{k_{RD}^2}. \end{cases} \tag{22}$$

Substituting (21) and (22) into (14), we obtain $F(x)$ of the considered MIMO-FDR system as

$$F(x) = \begin{cases} 1 - \exp\left(-\dfrac{\Theta x}{1-k_{SR}^2 x} - \dfrac{\Psi x}{1-k_{RD}^2 x}\right)\displaystyle\sum_{i=0}^{N_r-1}\sum_{j=0}^{N_t-1}\frac{1}{i!j!}\left(\frac{\Theta x}{1-k_{SR}^2 x}\right)^i\left(\frac{\Psi x}{1-k_{RD}^2 x}\right)^j, & x < \dfrac{1}{\lambda^2}, \\ 1, & x \geqslant \dfrac{1}{\lambda^2}, \end{cases} \tag{23}$$

where $\frac{1}{\lambda^2} = \min\left(\frac{1}{k_{RD}^2}, \frac{1}{k_{SR}^2}\right)$.

Replacing $F(x)$ in (23) into (9), we have

$$\begin{aligned} \mathrm{SER} &= \frac{a\sqrt{b}}{2\sqrt{2\pi}}\int_0^\infty \frac{\exp\left(-\frac{bx}{2}\right)}{\sqrt{x}}F(x)dx \\ &= \frac{a\sqrt{b}}{2\sqrt{2\pi}}\left[\int_0^{\frac{1}{\lambda^2}}\frac{\exp\left(-\frac{bx}{2}\right)}{\sqrt{x}}\left(1-\exp\left(-\frac{\Theta x}{1-k_{SR}^2 x}-\frac{\Psi x}{1-k_{RD}^2 x}\right)\sum_{i=0}^{N_r-1}\sum_{j=0}^{N_t-1}\frac{1}{i!j!}\left(\frac{\Theta x}{1-k_{SR}^2 x}\right)^i\left(\frac{\Psi x}{1-k_{RD}^2 x}\right)^j\right)dx \right. \\ &\qquad \left. + \int_{\frac{1}{\lambda^2}}^\infty \frac{\exp\left(-\frac{bx}{2}\right)}{\sqrt{x}}dx\right] \end{aligned} \tag{24}$$

$$\begin{aligned} &= \frac{a\sqrt{b}}{2\sqrt{2\pi}}\left[\int_0^\infty \frac{\exp\left(-\frac{bx}{2}\right)}{\sqrt{x}}dx - \sum_{i=0}^{N_r-1}\sum_{j=0}^{N_t-1}\frac{1}{i!j!}\int_0^{\frac{1}{\lambda^2}}\frac{\exp\left(-\frac{bx}{2}-\frac{\Theta x}{1-k_{SR}^2 x}-\frac{\Psi x}{1-k_{RD}^2 x}\right)}{\sqrt{x}}\left(\frac{\Theta x}{1-k_{SR}^2 x}\right)^i\left(\frac{\Psi x}{1-k_{RD}^2 x}\right)^j dx\right] \\ &= \frac{a\sqrt{b}}{2\sqrt{2\pi}}\left[\int_0^\infty \frac{\exp\left(-\frac{bx}{2}\right)}{\sqrt{x}}dx - \sum_{i=0}^{N_r-1}\sum_{j=0}^{N_t-1}\frac{\Theta^i\Psi^j}{i!j!}\int_0^{\frac{1}{\lambda^2}}\frac{x^{i+j-\frac{1}{2}}\exp\left(-\frac{bx}{2}-\frac{\Theta x}{1-k_{SR}^2 x}-\frac{\Psi x}{1-k_{RD}^2 x}\right)}{(1-k_{SR}^2 x)^i(1-k_{RD}^2 x)^j}dx\right]. \end{aligned} \tag{25}$$

Using [51, Eq. (3.361.2)], the first integral in (25) is calculated as

$$\int_0^\infty \frac{\exp\left(-\frac{bx}{2}\right)}{\sqrt{x}}dx = \sqrt{\frac{2\pi}{b}}. \tag{26}$$

Based on [52, Eq. (25.4.30)], the second integral in (25) is computed as

Table 2
Parameters for the system performance evaluation.

Notations	Description	Fixed value	Varying range
SNR	Signal-to-noise ratio	40 dB	0→40dB
σ^2	Variance of Gaussian noise	1	none
(a,b)	Modulation types	$(2,1)$	$(1,2),(\frac{1}{\sqrt{2}},\frac{3}{7})$
σ_e^2	Variance of channel estimation error	0.01	0→0.3
k	HI level	0.15	0.05→0.3
l	RSI level	0.15	0→0.3
N_r	Number of reception antennas of R	4	2, 3, 5, 6
N_t	Number of transmission antennas of R	4	6, 5, 3, 2
hline			

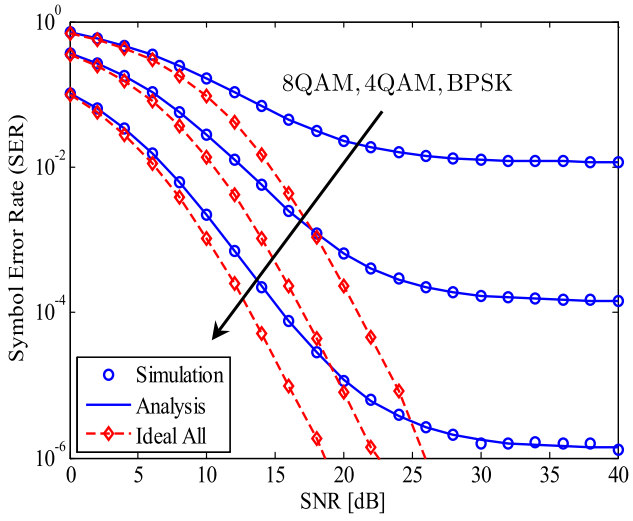

Fig. 2. SER of the considered MIMO-FDR system versus the average SNR for different modulation schemes, $N_t = N_r = 4, \sigma_e^2 = 0.01, k = 0.15$, and $l = 0.15$.

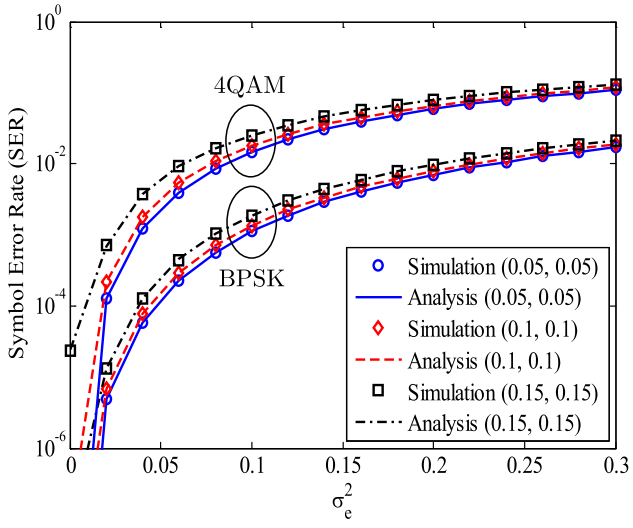

Fig. 3. SER of the considered MIMO-FDR system versus the channel estimation error for different values of HI and RSI levels, SNR = 40dB, BPSK and 4QAM modulations.

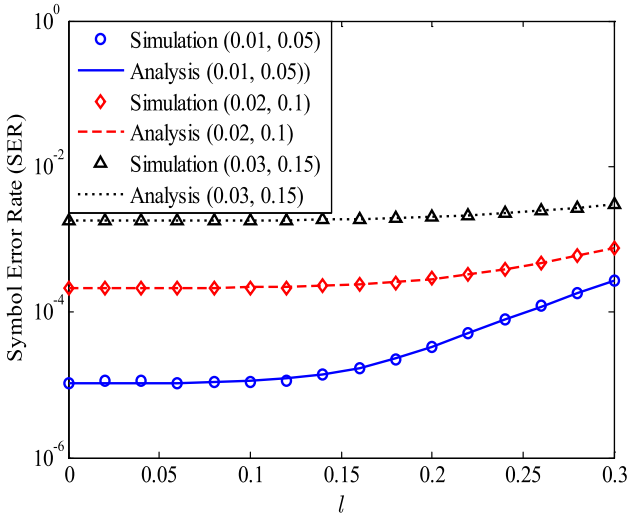

Fig. 4. Impact of RSI level l on the SER of the considered MIMO-FDR system using 4QAM modulation for different values of σ_e^2, and k, SNR = 40dB.

$$\int_0^{\frac{1}{\lambda^2}} \frac{x^{i+j-\frac{1}{2}} \exp\left(-\frac{bx}{2} - \frac{\Theta x}{1-k_{SR}^2 x} - \frac{\Psi x}{1-k_{RD}^2 x}\right)}{(1-k_{SR}^2 x)^i (1-k_{RD}^2 x)^j} dx$$

$$= \frac{\pi}{2M\lambda^2} \sum_{m=1}^{M} \frac{\left(\frac{1}{2\lambda^2}(1+\phi_m)\right)^{i+j-\frac{1}{2}} \sqrt{1-\phi_m^2}}{\left(1-\frac{k_{SR}^2}{2\lambda^2}(1+\phi_m)\right)^i \left(1-\frac{k_{RD}^2}{2\lambda^2}(1+\phi_m)\right)^j}$$

$$\times \exp\left(-\frac{b(1+\phi_m)}{4\lambda^2} - \frac{\Theta(1+\phi_m)}{2\lambda^2 - k_{SR}^2(1+\phi_m)} - \frac{\Psi(1+\phi_m)}{2\lambda^2 - k_{RD}^2(1+\phi_m)}\right)$$

$$= \frac{\pi}{2M\lambda^2} \sum_{m=1}^{M} \frac{\Lambda^{i+j-\frac{1}{2}} \sqrt{1-\phi_m^2}}{(1-k_{SR}^2\Lambda)^i (1-k_{RD}^2\Lambda)^j} \exp\left(-\frac{b\Lambda}{2} - \frac{\Theta\Lambda}{1-k_{SR}^2\Lambda} - \frac{\Psi\Lambda}{1-k_{RD}^2\Lambda}\right), \quad (27)$$

where $\Lambda = \frac{1}{2\lambda^2}(1+\phi_m)$ and $\phi_m = \cos\left(\frac{(2m-1)\pi}{2M}\right)$.

Replacing (26) and (27) into (25), we obtain the SER of the

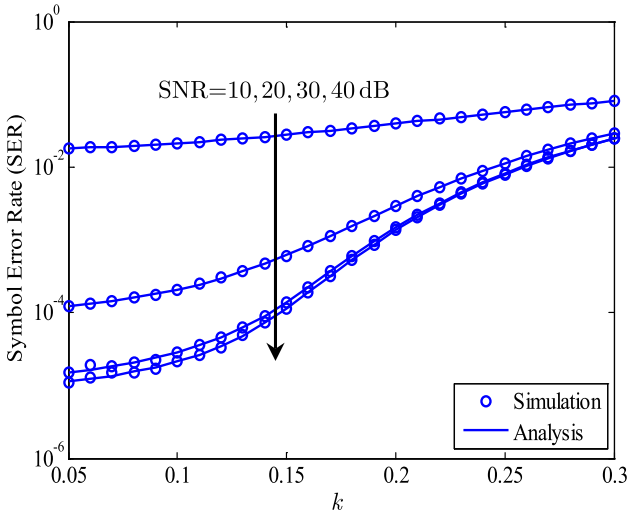

Fig. 5. SER of the considered MIMO-FDR system versus THI level k for different values of SNR, $\sigma_e^2 = 0.01, l = 0.1$.

considered system as in (10). The proof is complete.

It is also noted that approximating the SER expression in (10) in extreme conditions can cause a big gap between the analysis result and simulation result due to the properties of this expression. Therefore, the asymptotic form of the SER is not provided in this paper.

4. Numerical Results and Discussions

In this section, we evaluate the SER of the considered MIMO-FDR system by using mathematical analysis in previous section. Particularly, the SER of the MIMO-FDR system with CEE, THI and RSI is compared with that of the system in the case of all ideal factors (perfect CSI, transceiver hardwares and SIC) or one factor is ideal (perfect CSI or perfect hardwares or perfect SIC). The parameter settings in all scenarios are chosen as $P_{\rm S} = P_{\rm R} = P; \sigma_{\rm R}^2 = \sigma_{\rm D}^2 = \sigma^2; \Omega_{\rm SR} = \Omega_{\rm RD} = 1; \sigma_{e_{\rm SR}}^2 = \sigma_{e_{\rm RD}}^2 = \sigma_e^2; k_{\rm S}^{\rm t} = k_{\rm R}^{\rm r} = k_{\rm R}^{\rm t} = k_{\rm D}^{\rm r} = k$. The average SNR is computed as ${\rm SNR} = P/\sigma^2$. For the sake of clarity, some parameters along with their values are listed in Table 2.

Fig. 2 illustrates the SER of the considered MIMO-FDR system versus the average SNR for different modulation schemes, i.e., BPSK $((a,b) = (1,2))$, 4QAM $((a,b) = (2,1))$, and 8QAM $((a,b) = (4-\sqrt{2}, 3/7))$. The SER in the case of $\sigma_e^2 = 0.01, k = 0.15$, and $l = 0.15$ is compared with that in the case of ideal all $(\sigma_e^2 = k = l = 0)$. In Fig. 2, the analysis curves are plotted by using (10) while the markers denote the Monte-Carlo simulation results. It is clear from Fig. 2 that, the impacts of CEE, THI, and RSI are stronger in high SNR regime. Particularly, in the low SNR regime (SNR$\leqslant$10 dB), SERs in the case of CEE, THI, and RSI are similar to those in the case of all ideal factors for three modulation schemes. However, in high SNR regime (SNR $>$ 10 dB), they are significantly different. Especially, SERs in the case of CEE, THI, and RSI go to the error floors at SNR = 30 dB while SERs in the case of all ideal factors still go down fast when SNR increases. In the error floor, SERs are approximate 10^{-6}, 10^{-4}, and 4×10^{-3} for BPSK, 4QAM, and 8QAM modulation schemes, respectively. In contrast, SERs in the case of all ideal factors are 10^{-6} when SNR = 19, 23, and 25 dB for BPSK, 4QAM, and 8QAM modulation schemes, respectively. Those results demonstrate the great impacts of CEE, THI, and RSI on the SER of the considered system. Note that the SERs in the case of CEE, THI, and RSI reach the error floors in high SNR regime because the SINDRs at R and D are constants in high SNR regime.[2]

Fig. 3 presents the effect of channel estimation error σ_e^2 on the SER of the considered MIMO-FDR system for different values of THI level k and RSI level l. The dyad $(.,.)$ in Fig. 3 is used to show the values of k and l. For example, $(0.05, 0.05)$ means $k = 0.05$ and $l = 0.05$. Note that in the case of $\sigma_e^2 = 0$, we obtain SER of the system with perfect CSI. Fig. 3 shows a strong effect of CEE on the SER of the considered system. For BPSK modulation and three values of THI and RSI levels, i.e., $(0.05, 0.05)$, $(0.1, 0.1)$, and $(0.15, 0.15)$, SER $= 10^{-6}$ when $\sigma_e^2 = 0.02$, meanwhile SER $= 10^{-4}$ when $\sigma_e^2 = 0.04$. Thus, when CEE changes from 0.02 to 0.04, SER increases 100 times. In contrast, these SERs are nearly similar when THI and RSI levels change from 0.05 to 0.15. Additionally, with high values of σ_e^2 ($\sigma_e^2 \geqslant 0.15$), SER changes slowly and reaches error floor. On the other hand, we see that THI and RSI's effects are more significant for high data transmission rates. In particular, the difference between the cases of $(0.05, 0.05)$ and $(0.15, 0.15)$ for 4QAM is larger than that for BPSK, especially with the small values of σ_e^2. We should note that the average SNR at the relay and destination in practice may be lower than 40 dB. However, to clearly show the system behavior under the effects of CEE, THI, and RSI, we set the average SNR up to 40 dB.

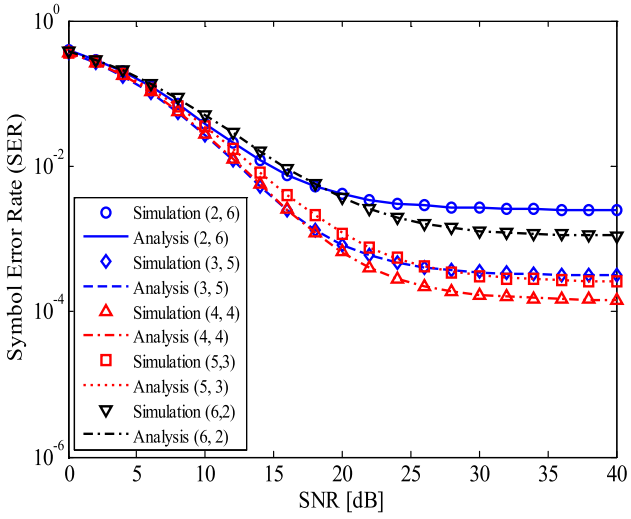

Fig. 6. SER of the considered MIMO-FDR system versus the average SNR for different numbers of receiving and transmitting antennas at R.

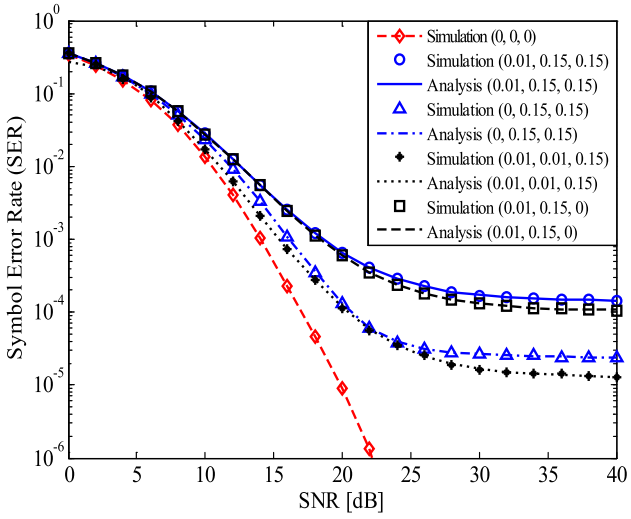

Fig. 7. The impacts of three or couple factors on SER of the considered system with $N_{\rm r} = N_{\rm t} = 4$.

Fig. 4 shows the impact of RSI level l on the SER of the considered MIMO-FDR system using 4QAM modulation for different values of σ_e^2 and k. The dyad $(.,.)$ in Fig. 4 denotes the values of σ_e^2 and k. It is obvious from Fig. 4, in the case of high σ_e^2 and k, i.e., $(0.02, 0.1)$ and $(0.03, 0.15)$, the SER of the considered system is nearly unchanged when l varies from 0 to 0.3. It is because, with these values of σ_e^2 and k, SER nearly reaches the error floor. Thus, SER approximates a constant, although the RSI level is changed from $l = 0$ (perfect SIC) to $l = 0.3$ (imperfect SIC). However, in the case of small σ_e^2 and k, i.e., $(0.01, 0.05)$, the effect of l on SER is significant, especially when $l \geqslant 0.15$. As a result, besides applying all SIC techniques for FD transmission mode, various solutions to reduce the amount of CEE and THI need to be studied and exploited further to reduce the SER of the considered MIMO-FDR system.

Fig. 5 examines the impact of THI level k on the SER of the considered MIMO-FDR system. It should be noticed that, due to the fraction $1/k_{\rm SR}^2$ and $1/k_{\rm RD}^2$, k cannot be set from 0 such as σ_e^2 and l. We can see that the effect of k is stronger for high values of SNR. Specifically, when

[2] Specifically, for the investigated parameters, the SINDRs at R and D given by (6) and (7) in high SNR regime, respectively, become

$$\lim_{\rm SNR\to\infty} \gamma_{\rm R} = \frac{N_{\rm r}}{N_{\rm r} k_{\rm SR}^2 + \sigma_{e_{\rm SR}}^2 (1 + k_{\rm SR}^2) + l^2}, \text{ and } \lim_{\rm SNR\to\infty} \gamma_{\rm D} = \frac{N_{\rm t}}{N_{\rm t} k_{\rm RD}^2 + N_{\rm t} \sigma_{e_{\rm RD}}^2 (1 + k_{\rm RD}^2)}.$$

SNR = 10 dB, SER changes from 10^{-2} to 10^{-1} when k ranges from 0.05 to 0.3. In other words, SER increases ten times within this range of k. However, when SNR = 20 dB, SER increases from 10^{-4} to 4×10^{-2}, that means it increases 400 times for that range of k. For higher SNR values, i.e., SNR = 30, 40 dB, SER increases 4000 times for that range of k. Also, for a certain value of k, the SER significantly reduces when the SNR increases from 10 dB to 20 dB. However, this reduction is small when the SNR increases from 30 dB to 40 dB. It is because within this high SNR regime, the SINDRs at R and D increase slowly (refer to (6), (7), and Fig. 2). Combining both Fig. 2 and Fig. 5, we can see that, depending on the requirements of wireless systems and the values of CEE, THI, and RSI levels, the suitable transmission power of source and relay can be selected to save energy and reduce the impacts of CEE, THI, and RSI. For example, high transmission power, such as SNR = 50 dB, should not be used because using high transmission power may cause a larger THI level. Also, high transmission power as SNR = 50 dB cannot reduce SER since the error floor appears even when SNR⩽40 dB.

Fig. 6 investigates the SER of the considered system versus the average SNR for different numbers of receiving and transmitting antennas of R. We consider the case that $N_r + N_t = 8$. In Fig. 6, the dyad $(.,.)$ denotes the number of receiving and transmitting antennas of R. For an example, $(2, 6)$ denotes $N_r = 2$ and $N_t = 6$ antennas. As can be seen from Fig. 6, the case $N_r = N_t = 4$ is the best among five investigated cases. In contrast, the case $N_r = 2, N_t = 6$ is the worst. These results are perfectly reasonable for the considered MIMO-FDR system. It is because R exploits FD transmission mode; thus, the SINDR at R is influenced by the RSI. Therefore, when a larger number of transmitting antennas of R is used, the RSIs at the receiving antennas become stronger. In contrast, a small number of transmitting antennas and a large number of receiving antennas of R can greatly reduce the RSI power; however, the R–D link is worse than S–R link. Consequently, the SER of $(6, 2)$ is better than that of $(2, 6)$, but these SERs are worse than those of $(5, 3)$ or $(3, 5)$. Hence, we should use $N_r = N_t$ at the relay for the considered system to reach the lowest SER.

Fig. 7 considers the impacts of three or couple factors on SER of the considered system. The triad $(.,.,.)$ in Fig. 7 denotes σ_e^2, k, and l. For example, $(0.01, 0.15, 0)$ means $\sigma_e^2 = 0.01, k = 0.15$, and $l = 0$. For the investigated values of σ_e^2, k, and l, the impacts of σ_e^2 and k are remarkable. As can be seen from Fig. 7, the SER in the case of $(0.01, 0.15, 0)$ approximates to the SER in the case of $(0.01, 0.15, 0.15)$. In other words, although RSI level changes from 0.15 to 0, the SER is nearly unchanged. This result indicates that when CEE and THI are large enough, the impact of RSI can be neglected. On the other hand, when σ_e^2 varies from 0.01 to 0 (the cases of $(0.01, 0.15, 0.15)$ and $(0, 0.15, 0.15)$) or k varies from 0.15 to 0.01 (the cases of $(0.01, 0.15, 0.15)$ and $(0.01, 0.01, 0.15)$), SER significantly reduces. These results emphasize the great effects of CEE and THI on the SER of the considered system. Therefore, all solutions for reducing CEE and THI levels need to developed together with SIC technique to improve the performance of MIMO-FDR system.

5. Conclusion

In practice, besides the RSI, MIMO-FDR systems are also affected by various negative parameters such as channel estimation error and transceiver hardware impairments. In this paper, we mathematically derived the exact closed-form expression of SER under the impacts of CEE, THI, and RSI to evaluate the MIMO-FDR system's performance in realistic scenarios. Under the effects of three negative factors, SER of the considered MIMO-FDR system goes to the error floor in the high SNR regime. Furthermore, the impacts of one or two factors on SER were also investigated to get more insights into the SER performance of the considered MIMO-FDR system. Numerical results indicate that the impact of CEE is most substantial among three negative factors. Additionally, when two factors are large enough, the effect of the other factor can be neglected. Therefore, besides proposing solutions and algorithms for SIC in FD transmission mode, more efforts are required to get the smallest values of channel estimation error and transceiver hardware impairments so that the performance of the considered MIMO-FDR system is enhanced.

Declaration of Competing Interest

The authors declare that they have no known competing financial interests or personal relationships that could have appeared to influence the work reported in this paper.

Appendix A. Supplementary material

Supplementary data associated with this article can be found, in the online version, at https://doi.org/10.1016/j.aeue.2021.153751.

References

[1] Cai Y, Xu Y, Shi Q, Champagne B, Hanzo L. Robust joint hybrid transceiver design for millimeter wave full-duplex MIMO relay systems. IEEE Trans. Wirel. Commun. 2019;18(2):1199–215.

[2] Tam HHM, Tuan HD, Nasir AA, Duong TQ, Poor HV. MIMO energy harvesting in full-duplex multi-user networks. IEEE Trans. Wirel. Commun. 2017;16(5):3282–97.

[3] Coskun AF, Kucur O. Performance analysis of maximal-ratio transmission/receive antenna selection in nakagami-m fading channels with channel estimation errors and feedback delay. IEEE Trans. Veh. Technol. 2012;61(3):1099–108.

[4] Rui X. Analysis of MIMO MRT/SC systems. Wirel. Pers. Commun. 2012;62(1):117–26.

[5] Qin D, Wang Y, Zhou T. Performance analysis of AF relays with maximal ratio combining in nakagami-m fading environments. Wirel. Commun. Mob. Comput. 2019;2019:1–11.

[6] Darabkh KA, Amro OM, Salameh HB, Al-Zubi RT. A-Z overview of the in-band full-duplex cognitive radio networks. Comput. Commun. 2019;145:66–95.

[7] Alsaba Y, Leow CY, Rahim SKA. Full-duplex cooperative non-orthogonal multiple access with beamforming and energy harvesting. IEEE Access 2018;6:19726–38.

[8] Gazestani AH, Ghorashi SA, Mousavinasab B, Shikh-Bahaei M. A survey on implementation and applications of full duplex wireless communications. Phys. Commun. 2019;34:121–34.

[9] Deng Y, Kim KJ, Duong TQ, Elkashlan M, Karagiannidis GK, Nallanathan A. Full-duplex spectrum sharing in cooperative single carrier systems. IEEE Trans. Cogn. Commun. Netw. 2016;2(1):68–82.

[10] Doan X, Nguyen N, Yin C, da Costa DB, Duong TQ. Cognitive full-duplex relay networks under the peak interference power constraint of multiple primary users. EURASIP J. Wirel. Commun. Netw. 2017;2017:8.

[11] Ahmed E, Eltawil AM. All-digital self-interference cancellation technique for full-duplex systems. IEEE Trans. Wirel. Commun. 2015;14(7):3519–32.

[12] Bharadia D, McMilin E, Katti S. Full duplex radios. In: Chiu DM, Wang J, Barford P, Seshan S, editors. ACM SIGCOMM 2013 Conference. SIGCOMM'13, Hong Kong, China, August 12–16, 2013, ACM; 2013. p. 375–86.

[13] Everett E, Sahai A, Sabharwal A. Passive self-interference suppression for full-duplex infrastructure nodes. IEEE Trans. Wirel. Commun. 2014;13(2):680–94.

[14] Hong SS, Brand J, Choi JI, Jain M, Mehlman J, Katti S, Levis P. Applications of self-interference cancellation in 5g and beyond. IEEE Commun. Mag. 2014;52(2):114–21.

[15] Irio L, Oliveira R. Distribution of the residual self-interference power in in-band full-duplex wireless systems. IEEE Access 2019;7:57516–26.

[16] Abbasi O, Ebrahimi A. Cooperative NOMA with full-duplex amplify-and-forward relaying. Trans. Emerg. Telecommun. Technol. 2018;29(7):1–15.

[17] Nguyen BC, Tran XN, Hoang TM, et al. Performance analysis of full-duplex vehicle-to-vehicle relay system over double-rayleigh fading channels. Mobile Networks and Applications 2020;25(1):363–72.

[18] Kolodziej KE, Perry BT, Herd JS. In-band full-duplex technology: Techniques and systems survey. IEEE Trans. Microw. Theory Tech. 2019;67(7):3025–41.

[19] Nguyen BC, Hoang TM, Tran PT, Nguyen TN. Outage probability of NOMA system with wireless power transfer at source and full-duplex relay. AEU-International Journal of Electronics and Communications 2020;116:152957.

[20] Nguyen LV, Nguyen BC, Tran XN, Dung LT. Closed-form expression for the symbol error probability in full-duplex spatial modulation relay system and its application in optimal power allocation. Sensors 2019;19(24):5390.

[21] Cao NB, Hoang TM, Dung LT. Performance analysis of vehicle-to-vehicle communication with full-duplex amplify-and-forward relay over double-rayleigh fading channels. Veh. Commun. 2019;19:1–9.

[22] Cao NB, Hoang TM, Pham XN, Tran PT. Performance analysis of energy harvesting-based full-duplex decode-and-forward vehicle-to-vehicle relay networks with nonorthogonal multiple access. Wirel. Commun. Mob. Comput. 2019;2019:1–11.

[23] Narayanan S, Ahmadi H, Flanagan MF. On the performance of spatial modulation MIMO for full-duplex relay networks. IEEE Trans. Wirel. Commun. 2017;16(6):3727–46.

[24] Nguyen BC, Kieu TN, Hoang TM, Tran PT, Voznák M. Analysis of MRT/MRC diversity techniques to enhance the detection performance for MIMO signals in

full-duplex wireless relay networks with transceiver hardware impairment. Phys. Commun. 2020;42:101132.
[25] Nguyen N, Ngo HQ, Duong TQ, Tuan HD, da Costa DB. Full-duplex cyber-weapon with massive arrays. IEEE Trans. Commun. 2017;65(12):5544–58.
[26] Nguyen LV, Nguyen BC, Tran XN, Dung LT. Transmit antenna selection for full-duplex spatial modulation multiple-input multiple-output system. IEEE Syst. J. 2020;14(4):4777–85.
[27] Cao NB, Tran XN. Performance analysis of full-duplex amplify-and-forward relay system with hardware impairments and imperfect self-interference cancellation. Wirel. Commun. Mob. Comput. 2019;2019:1–10.
[28] Choi D, Lee JH. Outage probability of two-way full-duplex relaying with imperfect channel state information. IEEE Commun. Lett. 2014;18(6):933–6.
[29] Li C, Wang H, Yao Y, Chen Z, Li X, Zhang S. Outage performance of the full-duplex two-way DF relay system under imperfect CSI. IEEE Access 2017;5:5425–35.
[30] Day BP, Margetts AR, Bliss DW, Schniter P. Full-duplex MIMO relaying: Achievable rates under limited dynamic range. IEEE J. Sel. Areas Commun. 2012;30(8):1541–53.
[31] Nguyen BC, Tran XN, Tran DT, Pham XN, Dung LT. Impact of hardware impairments on the outage probability and ergodic capacity of one-way and two-way full-duplex relaying systems. IEEE Trans. Veh. Technol. 2020;69(8):8555–67.
[32] Dey S, Sharma E, Budhiraja R. Scaling analysis of hardware-impaired two-way full-duplex massive MIMO relay. IEEE Commun. Lett. 2019;23(7):1249–53.
[33] González GJ, Gregorio FH, Cousseau JE, Riihonen T, Wichman R. Full-duplex amplify-and-forward relays with optimized transmission power under imperfect transceiver electronics. EURASIP J. Wirel. Commun. Netw. 2017;2017:76.
[34] Nguyen BC, Hoang TM, Tran PT. Improving the performance of spatial modulation full-duplex relaying system with hardware impairment using transmit antenna selection. IEEE Access 2020;8:20191–202.
[35] Tabataba FS, Sadeghi P, Hucher C, Pakravan MR. Impact of channel estimation errors and power allocation on analog network coding and routing in two-way relaying. IEEE Trans. Veh. Technol. 2012;61(7):3223–39.
[36] Li X, Tepedelenlioglu C, Senol H. Channel estimation for residual self-interference in full duplex amplify-and-forward two-way relays. IEEE Trans. Wireless Commun. 2017;16(8):4970–83.
[37] Li L, Dong C, Wang L, Hanzo L. Spectral-efficient bidirectional decode-and-forward relaying for full-duplex communication. IEEE Trans. Veh. Technol. 2016;65(9):7010–20.
[38] Li C, Chen Z, Wang Y, Yao Y, Xia B. Outage analysis of the full-duplex decode-and-forward two-way relay system. IEEE Trans. Veh. Technol. 2017;66(5):4073–86.
[39] Schenk T. RF imperfections in high-rate wireless systems. In: impact and digital compensation. Springer Science & Business Media; 2008.
[40] Björnson E, Hoydis J, Kountouris M, Debbah M. Massive MIMO systems with non-ideal hardware: Energy efficiency, estimation, and capacity limits. IEEE Trans. Inf. Theory 2014;60(11):7112–39.
[41] Bjornson E, Matthaiou M, Debbah M. A new look at dual-hop relaying: Performance limits with hardware impairments. IEEE Trans. Commun. 2013;61(11):4512–25.
[42] Papazafeiropoulos AK, Sharma SK, Ratnarajah T, Chatzinotas S. Impact of residual additive transceiver hardware impairments on rayleigh-product MIMO channels with linear receivers: Exact and asymptotic analyses. IEEE Trans. Commun. 2018;66(1):105–18.
[43] Dardari D, Tralli V, Vaccari A. A theoretical characterization of nonlinear distortion effects in OFDM systems. IEEE Trans. Commun. 2000;48(10):1755–64.
[44] Schenk TCW, Fledderus ER, Smulders PFM. Performance analysis of zero-if MIMO OFDM transceivers with IQ imbalance. J. Commun. 2007;2(7):9–19.
[45] Zetterberg P. Experimental investigation of TDD reciprocity-based zero-forcing transmit precoding. EURASIP J. Adv. Signal Process. 2011;2011:1–10.
[46] Holma H, Toskala A. LTE for UMTS: Evolution to LTE-advanced. John Wiley & Sons; 2011.
[47] Kyritsi P, Valenzuela RA, Cox DC. Channel and capacity estimation errors. IEEE Commun. Lett. 2002;6(12):517–9.
[48] Li S, Yang K, Zhou M, Wu J, Song L, Li Y, Li H. Full-duplex amplify-and-forward relaying: Power and location optimization. IEEE Trans. Veh. Technol. 2017;66(9):8458–68.
[49] Goldsmith A. Wireless communications. Cambridge University Press; 2005.
[50] Yilmaz A, Kucur O. Performance of transmit antenna selection and maximal-ratio combining in dual hop amplify-and-forward relay network over nakagami-m fading channels. Wirel. Pers. Commun. 2012;67(3):485–503.
[51] Jeffrey A, Zwillinger D. Table of integrals, series, and products. Academic Press; 2007.
[52] Abramowitz M, Stegun IA. Handbook of mathematical functions with formulas, graphs, and mathematical tables, Vol. 9. New York: Dover; 1972.